Semi-exclusive production of photons at HERA

P. Hoyer[1], M. Maul[2], A. Metz[3]

[1] NORDITA, Blegdamsvej 17, 2100 Copenhagen, Denmark
[2] Department of Theoretical Physics, Lund University, Sölvegatan 14 a, 223 62 Lund, Sweden
[3] DAPNIA/SPhN, CEA-Saclay, 91191 Gif-sur-Yvette, France

Abstract. We study the feasibility of measuring the semi-exclusive photon production $\gamma + p \to \gamma + Y$ at HERA. The cross section of photons produced at large transverse momenta, recoiling off an inclusive system Y of limited mass, can without photon isolation cuts simply be expressed in terms of hard PQCD subprocesses and standard target parton distributions. With the help of event generators we identify the kinematic region where quark and gluon fragmentation processes can be neglected. The cross section in this semi-exclusive region is large enough to be measured with an upgraded HERA luminosity of $\mathcal{L} = 100\,\mathrm{pb}^{-1}$. The subprocesses of lowest order in α_s are suppressed at low recoil masses M_Y, compared to higher order gluon exchange, i.e. BFKL contributions. The distinct M_Y-dependence makes it possible to determine experimentally the kinematic range where the higher order processes dominate.

1. Introduction

Semi-exclusive reactions of the type $A + B \to C + Y$, where particle C emerges with large transverse momentum and the mass of the inclusive system Y satisfies $\Lambda_{\mathrm{QCD}} \ll M_Y \ll E_{\mathrm{cm}}$, provide a new tool for probing the structure of hadrons [1]. It is analogous to DIS, $ep \to eX$, in the sense that particles A and C form an effective current which probes the target B at large momentum transfer $t = (p_A - p_C)^2$, producing the inclusive system Y. Semi-exclusive cross sections factorize into a calculable short distance interaction times a standard target parton (b) distribution $f_{b/B}(x_S, -t)$ according to

$$\frac{\mathrm{d}\sigma}{\mathrm{d}t\mathrm{d}x_S}(A+B \to C+Y) = \sum_b f_{b/B}(x_S, -t)\frac{\mathrm{d}\sigma}{\mathrm{d}t}(Ab \to Cd),$$

(1)

where

$$x_s = -t/(M_Y^2 - t)$$

(2)

and the momentum transfer $-t$ serves as a factorization scale. For large $-t$ only compact configurations of particles A and C participate in the reaction, and their reinteractions with the target are suppressed. The final parton(s) d merges with the target spectators to form the inclusive system Y (Fig. 1a).

We shall discuss the feasibility of measuring semi-exclusive photon photoproduction, $\gamma p \to \gamma Y$ at HERA. Here the incoming and outgoing photons *together* form an effective current which probes a parton (quark or gluon) in the target with resolution $-t$ (Fig. 1a). This picture is valid provided that the final photon emerges isolated from

all hadrons in the inclusive system Y, which is ensured by the kinematic requirement $W^2/M_Y^2 \gg 1$, where W is the total γp center of mass energy, and M_Y is the mass of the hadronic system Y. Scattering on a single parton implies a large $-t$, typically of order M_Y^2. As we shall see, luminosity limitations impose $-t \ll M_Y^2$ at HERA, implying a small x_s in (2).

It is not a priori obvious how stringent the kinematic restrictions need to be to ensure semi-exclusive dynamics. At moderate W^2/M_Y^2, photons may be produced via parton fragmentation, following a hard process like $\gamma q \to gq$ (Fig. 1b). Such a process will typically generate hadrons comoving with the photon, implying $W^2/M_Y^2 \sim 1$. Depending on the probability that the photon takes most of the momentum of the fragmenting parton, such processes can nevertheless be significant at moderate values of W^2/M_Y^2. Based on the PYTHIA [2] and LUCIFER [3] Monte Carlo generators we conclude that fragmentation processes are insignificant for $W^2/M_Y^2 \gtrsim 10$ and $-t \gtrsim 4\,\mathrm{GeV}^2$.

Resolved photon contributions (Fig. 1c) are analogously suppressed since hadrons in the beam direction must carry little energy for W^2/M_Y^2 to be large. This requires the beam parton to carry nearly all the photon energy, and not to emit collinear bremsstrahlung prior to its hard scattering. The pointlike photon component transfers the full beam energy into the hard process and will thus dominate at large W^2/M_Y^2 and $-t$.

We also estimate the contribution of the Bethe–Heitler process (Fig. 1d), where the beam photon is virtual and the final photon is emitted from the electron. This process is typically detected because of the large angle recoil of
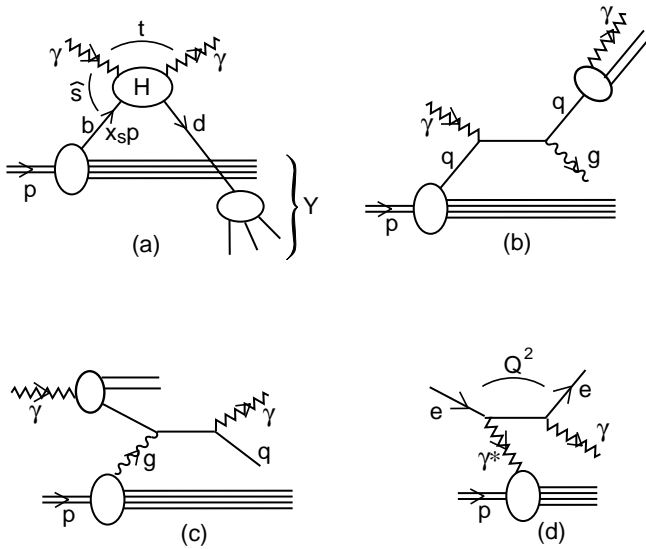
Fig. 1. **a** Semi-exclusive photoproduction of photons. The hard process H is calculable in PQCD. **b** Photons produced via parton fragmentation are accompanied by comoving hadrons. **c** The resolved photon leaves remnant hadrons in the beam direction. **d** The Bethe–Heitler process is not enhanced at low momentum transfer Q^2 between the electrons

Fig. 2a–c. Compton scattering subprocesses: Low order scattering on a quark **a** and on a gluon **b**. At high $\hat{s}/-t$, higher order amplitudes like **c** dominate, due to gluon exchange in the t-channel

the electron. We find that the Bethe–Heitler process is in any case negligible for invariant momentum transfers $Q^2 \lesssim 0.1$ GeV^2 between the initial and final electrons.

HERA data [4,5] on photon production at large transverse momentum have previously been compared with QCD calculations [6–8] in terms of an isolation cut [9–11], which imposes low accompanying transverse energy in a cone around the photon direction. Such a cut removes a large fraction of the photons produced by parton fragmentation, but allows resolved photon contributions. The isolation procedure requires modeling the non-perturbative fragmentation process. This is avoided for the semi-exclusive cross section (1), which depends only on standard structure functions and perturbatively calculable quantities.

Low order PQCD subprocess amplitudes which contribute to the hard vertex H of Fig. 1a are shown in Fig. 2. It is important to notice that the lowest order contributions of Figs. 2a,b actually are suppressed in the Regge limit $\hat{s} = x_s W^2 \to \infty$ at fixed (but large) $-t$, which is relevant for semi-exclusive dynamics. A (dimensionless) amplitude involving the exchange of two particles of spins j_1 and j_2 in the t-channel behaves in the Regge limit as $\sim (\hat{s}/-t)^\alpha$, where $\alpha = j_1 + j_2 - 1$. Hence the contribution of Fig. 2b, with $j_1 = j_2 = 1/2$, has $\alpha = 0$. The amplitude of Fig. 2a also has $\alpha = 0$. On the other hand, the higher order amplitude of Fig. 2c has $j_1 = j_2 = 1$ and thus $\alpha = 1$. At even higher orders logarithmic corrections from repeated gluon ladders are expected to build up hard Pomeron exchange in the BFKL approximation, as has been studied extensively for the present process [12–15].

It is interesting to explore at what value of $\hat{s}/-t$ the higher order diagrams begin to dominate. We find that the
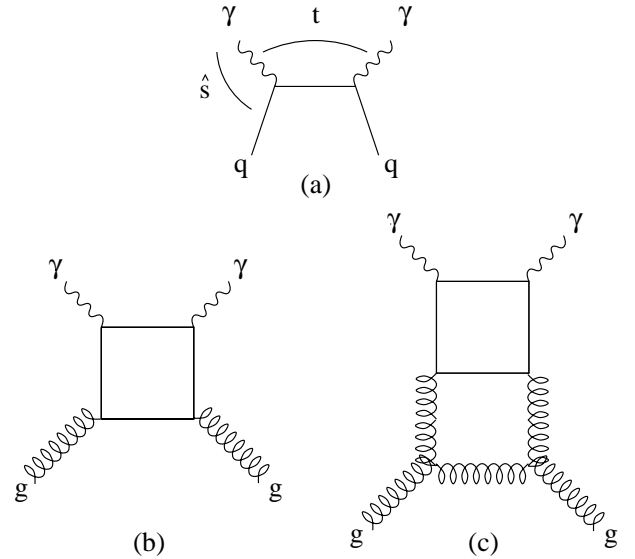
BFKL amplitude is numerically important compared to the lowest order contributions in the whole semi-exclusive range $\hat{s}/-t \gtrsim 10$. If the BFKL approximation is reliable (or the amplitude of Fig. 2c dominates) at such moderate values of the subprocess energy, then the subprocess cross section will be found to grow (or be constant) in this whole range. Alternatively, if the lowest order diagrams dominate, the subprocess cross section will decrease in the lower range of $\hat{s}/-t$. This would make it smaller than the BFKL estimate at high $\hat{s}/-t$.

2. Subprocess cross sections

The lowest order cross section for $\gamma q \to \gamma q$ (Fig. 2a) is [16]

$$\frac{\mathrm{d}\sigma_{\mathrm{LO}}}{\mathrm{d}t}(\gamma q \to \gamma q) = \frac{2\pi e_q^4 \alpha^2}{\hat{s}^2}\left(\frac{\hat{s}}{-\hat{u}} + \frac{-\hat{u}}{\hat{s}}\right), \qquad (3)$$

with $\alpha = e^2/4\pi$. For the lowest order $\gamma g \to \gamma g$ process (Fig. 2b) we have analogously [17,18],

$$\frac{\mathrm{d}\sigma_{\mathrm{LO}}}{\mathrm{d}t}(\gamma g \to \gamma g) = 2\left(\sum_q e_q^2\right)^2 \frac{\alpha^2 \alpha_{\mathrm{s}}^2}{64\pi \hat{s}^2}\left[|M_1(\hat{s},t,\hat{u})|^2\right.$$
$$+ \left.|M_1'(\hat{u},t,\hat{s})|^2 + |M_1'(t,\hat{s},\hat{u})|^2 + 20\right], \qquad (4)$$

where

$$|M_1(\hat{s},t,\hat{u})|^2 = \left(2 + 2\frac{t-\hat{u}}{\hat{s}}\ln\frac{t}{\hat{u}}\right.$$
$$+ \left.\frac{t^2+\hat{u}^2}{\hat{s}^2}\left[\ln^2\frac{t}{\hat{u}} + \pi^2\right]\right)^2,$$

$$|M_1'(\hat{u},t,\hat{s})|^2 = \left(2 + 2\frac{\hat{s}-t}{\hat{u}}\ln\frac{\hat{s}}{-t} + \frac{\hat{s}^2+t^2}{\hat{u}^2}\ln^2\frac{\hat{s}}{-t}\right)^2$$

$$+ 4\pi^2 \left(\frac{\hat{s}^2 + t^2}{\hat{u}^2} \ln \frac{\hat{s}}{-t} + \frac{\hat{s} - t}{\hat{u}} \right)^2 . \quad (5)$$

It is interesting to compare the size of the BFKL cross section to the LO ones given above. The $\gamma g \to \gamma g$ BFKL cross section is to leading logarithmic accuracy given by [13–15]

$$\frac{\mathrm{d}\sigma_{\mathrm{BFKL}}}{\mathrm{d}t}(\gamma g \to \gamma g) = \frac{81}{16} \frac{\alpha^2 \alpha_{\mathrm{s}}^4}{576 t^2} \pi \left(\sum_q e_q^2 \right)^2$$

$$\times \left[G \left(\frac{3\alpha_{\mathrm{s}}}{\pi} \ln \frac{\hat{s}}{-t} \right) \right]^2 ,$$

with

$$G(z) = \int_{-\infty}^{\infty} \frac{\mathrm{d}\nu}{1 + \nu^2} \frac{\nu^2}{\left(\nu^2 + \frac{1}{4}\right)^2} \frac{\tanh(\pi\nu)}{\pi\nu}$$

$$\times 2(11 + 12\nu^2) \exp\left[z\chi(\nu) \right] ,$$

$$\chi(\nu) = 2\psi(1) - 2\mathrm{Re} \left[\psi \left(\frac{1}{2} + \mathrm{i}\nu \right) \right] . \quad (6)$$

In Fig. 3 we show the dimensionless lowest order cross sections $\hat{s}^2 \mathrm{d}\sigma/\mathrm{d}t$ for $\gamma u \to \gamma u$ (solid line) and $\gamma g \to \gamma g$ (times 10, dot-dashed line). The small size of the lowest order $\gamma g \to \gamma g$ cross section means that it will be insignificant also in the physical process $\gamma N \to \gamma Y$, even though the gluon distribution is larger than the quark one at low values of x_s. The dashed line shows the BFKL cross section (6) for $\gamma g \to \gamma g$, based on iterating higher order diagrams like that in Fig. 2c. We used the fixed value $\alpha_{\mathrm{s}} = 0.2$ indicated by BFKL fits to HERA and Tevatron data [19–21]. The BFKL cross section is comparable to the lowest order one already at $\hat{s}/-t \simeq 10$, with their ratio growing roughly as $(\hat{s}/-t)^2$. It should be stressed, however, that the BFKL analysis is expected to be reliable only for $\hat{s}/-t \gtrsim 100$ [15], and that there may be sizable corrections from NLO corrections [22].

3. Semi-exclusive photon electroproduction at HERA

The $ep \to e\gamma Y$ electroproduction cross section is in the semi-exclusive limit $\Lambda_{\mathrm{QCD}}^2 \ll -t, M_Y^2 \ll W^2$ related to the subprocesses through

$$\frac{\mathrm{d}\sigma}{\mathrm{d}y \mathrm{d}t \mathrm{d}x_s}(ep \to e\gamma Y) =$$

$$f_{\gamma/e}(y, Q_{\mathrm{max}}^2) \sum_{i \in q,g} f_{i/p}(x_s, -t) \frac{\mathrm{d}\sigma}{\mathrm{d}t}(\gamma i \to \gamma i). \quad (7)$$

Here y is the fraction of momentum that the photon, of virtuality $\leq Q_{\mathrm{max}}^2$, takes of the electron beam. The Weizsäcker–Williams function $f_{\gamma/e}(y, Q_{\mathrm{max}}^2)$ is given in [23],

$$f_{\gamma/e}(y, Q_{\mathrm{max}}^2) = \frac{\alpha}{2\pi} \left[\frac{(1 + (1 - y)^2)}{y} \ln \frac{Q_{\mathrm{max}}^2 (1 - y)}{m_e^2 y^2} \right.$$

$$\left. + 2m_e^2 y \left(\frac{1}{Q_{\mathrm{max}}^2} - \frac{1 - y}{m_e^2 y^2} \right) \right] . \quad (8)$$

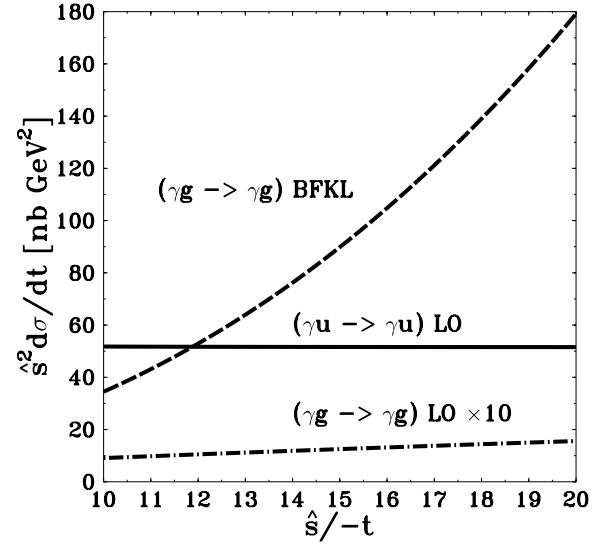**Fig. 3.** Lowest order subprocess cross sections $\hat{s}^2 \mathrm{d}\sigma/\mathrm{d}t$ for $\gamma u \to \gamma u$ (solid line) and $\gamma g \to \gamma g$ (times 10, dot-dashed line) for $10 \leq \hat{s}/-t \leq 20$. The dashed line shows the BFKL cross section extrapolated to this region of moderate subprocess energy, assuming $\alpha_{\mathrm{s}} = 0.2$. Three active flavors have been used in both the calculation of the process $\gamma g \to \gamma g$ to LO and the BFKL contribution

In our kinematical range the Weizsäcker–Williams scale is identical to the upper limit of the momentum transfer Q_{max}^2 between the electrons, as the hard scale $-t$, which characterizes the production process, is much larger than Q_{max}^2. A detailed discussion of the choice of the Weizsäcker–Williams scale can be found in [23,24]. For the parton distributions $f_{i/p}(x_s, -t)$ we use the GRV94 LO parameterizations [25].

In this section we first estimate the kinematic region in which the semi-exclusive production mechanism dominates, and then evaluate the physical cross section in this region.

3.1. Background from fragmentation and decay in photoproduction

Large transverse momentum photons can be produced through quark and gluon fragmentation $q, g \to \gamma + X$, following standard hard scattering processes such as photon gluon fusion, $\gamma g \to q\bar{q}$, and gluon bremsstrahlung, $\gamma q \to qg$. A second source of contributions are photons from hadronic decays like $\pi^0 \to \gamma\gamma$. In the following we call both background contributions "fragmentation". Such processes typically give hadrons in the photon direction, and are thus suppressed in the limit where $M_Y^2 \ll W^2$.

We have used the Monte Carlo event generators PYTHIA [2] and LUCIFER [3] to estimate the range of W^2/M_Y^2 in which semi-exclusive production dominates over fragmentation. These event generators include the direct (semi-exclusive) $\gamma q \to \gamma q$ cross section only at lowest order. As we observed in the introduction, the higher order contribution of Fig. 2c (and its possible BFKL en-
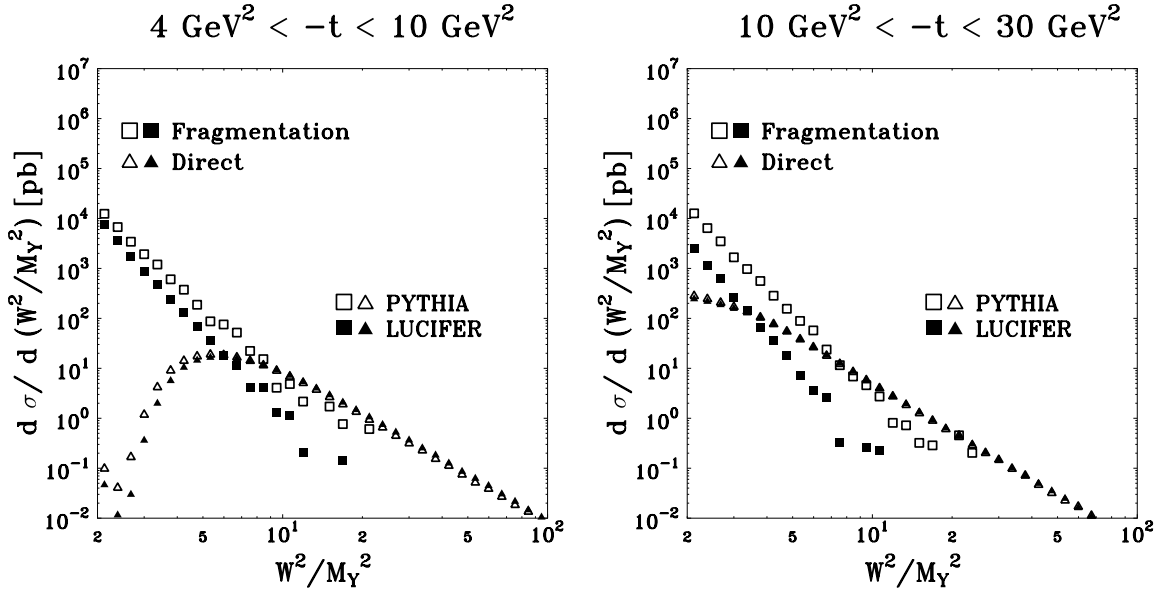
Fig. 4. Inclusive cross sections $\mathrm{d}\sigma(\gamma p \to \gamma Y)/\mathrm{d}(W^2/M_Y^2)$ for the photon with the largest E_γ^{CM} per event at $W = 200\,\mathrm{GeV}$. The t-range is $4\,\mathrm{GeV}^2 < -t < 10\,\mathrm{GeV}^2$ (left), and $10\,\mathrm{GeV}^2 < -t < 30\,\mathrm{GeV}^2$ (right). The triangles show the direct ($\gamma q \to \gamma q$) contribution of (3) and the squares show photons generated by fragmentation. The open squares and triangles are the result of the PYTHIA program and the filled squares and triangles are from the LUCIFER run. An additional cut $0.001 < x_s < 0.7$ has been applied in both figures. Higher order parton showering and resolved photon contributions are not included

hancement) actually dominates the lowest order process (Fig. 2a) at high $\hat{s}/-t$. Hence comparing the fragmentation background to only the LO semi-exclusive cross section gives a conservative estimate of the kinematic region where semi-exclusive dynamics dominates. It should also be kept in mind that the fragmentation contribution can be reduced with the help of photon isolation cuts [4,5, 9–11].

We evaluate the contributions from the direct process $\gamma q \to \gamma q$ and that from the background $\gamma g \to q\bar{q}$ and $\gamma q \to qg$ processes separately. If the final state contains several photons, we choose the one with largest energy E_γ^{CM} in the CM frame of the photon and the nucleon. The invariant mass M_Y^2 of the remaining particles is then given by $M_Y^2 = W^2 - 2W E_\gamma^{\mathrm{CM}}$.

In Fig. 4 we show the PYTHIA and LUCIFER results for $W = 200$ GeV and two ranges of photon transverse momentum, 4 GeV$^2 < -t < 10$ GeV^2 and 10 GeV$^2 < -t < 30$ GeV^2. It may be seen that the semi-exclusive process $\gamma q \to \gamma q$ starts to dominate for $W^2/M_Y^2 \gtrsim 10$. We have checked that the same conclusion holds for $W = 80$ GeV. Note that for $M_Y^2 \gg -t$, the subprocess variable $\hat{s}/-t$ of Fig. 3 is in the semi-exclusive limit simply related to W^2/M_Y^2,

$$\frac{W^2}{M_Y^2} = \frac{\hat{s}}{-t}\left(1 - \frac{t}{M_Y^2}\right) \simeq \frac{\hat{s}}{-t}. \qquad (9)$$

3.2. Background from the Bethe–Heitler process in electroproduction

When the incoming photon is virtual, the final photon may be radiated off the electron in the Bethe–Heitler (BH)
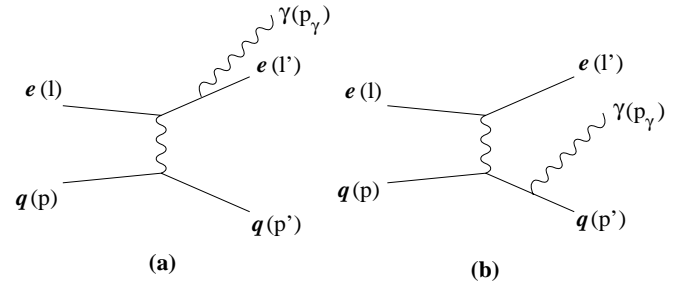

Fig. 5a,b. Sample diagrams for photon production via the Bethe–Heitler (BH) process **a** and virtual Compton scattering (VCS) **b**

process of Fig. 5a. We wish to determine the maximum value of Q^2 for which the BH cross section can be neglected compared to that of photon emission from the quark, i.e., the virtual Compton scattering (VCS) process of Fig. 5b.

At finite Q^2 the lowest order $ep \to e\gamma Y$ cross section can be written

$$\frac{\mathrm{d}\sigma_{\mathrm{LO}}(ep \to e\gamma Y)}{\mathrm{d}x_s \mathrm{d}W^2 \mathrm{d}Q^2 \, \mathrm{d}t \mathrm{d}\phi} = \frac{1}{2(4\pi)^4 x_s W_{ep}^4(\hat{s} + Q^2)}$$
$$\times \sum_q f_{q/p}(x_s, -t)\overline{|\mathcal{M}_q|^2}, \quad (10)$$

with

$$\overline{|\mathcal{M}_q|^2} = \overline{|\mathcal{M}_q^{\mathrm{VCS}}|^2} + \overline{|\mathcal{M}_q^{BH}|^2} + \overline{2\mathrm{Re}\left(\mathcal{M}_q^{BH}\mathcal{M}_q^{\mathrm{VCS}*}\right)}.$$

Here $Q^2 = -q^2 = -(l - l')^2$ and $\hat{s} = (q + p)^2 = x_s W_{\gamma p}^2$ in the notation of Fig. 5. ϕ is the angle between $\mathbf{q} \times \mathbf{p}_\gamma$ and $\ell \times \ell'$ with the three-vectors given in the CM frame of the

virtual photon and the proton, while $W_{ep} \approx 300$ GeV is the ep CM energy. We also define

$$\hat{s}_l = (l' + p_\gamma)^2, \quad \hat{u}_l = (l - p_\gamma)^2, \qquad (11)$$

which can be obtained from $\hat{s}$ and $\hat{u}$ by replacing the quark momentum $p(p')$ with the lepton momentum $l(l')$.

The squared VCS and BH matrix elements can now be written as

$$\overline{|\mathcal{M}_q^{\mathrm{VCS}}|^2} = \frac{-4(4\pi\alpha)^3 e_q^4}{Q^2 \hat{s}\hat{u}} F, \qquad (12)$$

$$\overline{|\mathcal{M}_q^{\mathrm{BH}}|^2} = \frac{4(4\pi\alpha)^3 e_q^2}{t\hat{s}_l\hat{u}_l} F, \qquad (13)$$

with the common factor F given by

$$
\begin{aligned}
F = {}& \hat{s}^2 + (\hat{s}+t)^2 + \hat{u}_l^2 + (2W_{eq}^2 + \hat{u}_l)^2 - 2\hat{s}(2W_{eq}^2 + \hat{u}_l) \\
& - 2t(W_{eq}^2 + \hat{u}_l) + 2Q^2(2\hat{s} + t - 3W_{eq}^2 - 2\hat{u}_l) + 3Q^4,
\end{aligned}
\qquad (14)
$$

and $W_{eq}^2 = (l+p)^2 = x_s W_{ep}^2$. We have

$$
\begin{aligned}
\overline{2\mathrm{Re}\left(\mathcal{M}_q^{\mathrm{BH}}\mathcal{M}_q^{\mathrm{VCS}*}\right)} = {}& \frac{8(4\pi\alpha)^3 e_q^3}{Q^2 t} \\
& \times \Bigg\{ Q^2 \left[-\frac{1}{2}(\hat{s}-\hat{u})\left(\frac{1}{\hat{s}_l}-\frac{1}{\hat{u}_l}\right) + \frac{1}{\hat{u}_l}(l\cdot p + l\cdot p') \right. \\
& + \frac{1}{\hat{s}_l}(l'\cdot p + l'\cdot p') \Bigg] \\
& + t\left[\frac{1}{2}(\hat{s}_l - \hat{u}_l)\left(\frac{1}{\hat{s}}-\frac{1}{\hat{u}}\right) - \frac{1}{\hat{u}}(l\cdot p + l'\cdot p) \right. \\
& - \frac{1}{\hat{s}}(l\cdot p' + l'\cdot p') \Bigg] \\
& - 8(l\cdot p\, l'\cdot p' + l\cdot p'\, l'\cdot p) \\
& \times \left(\frac{l\cdot p}{\hat{u}\hat{u}_l} + \frac{l\cdot p'}{\hat{s}\hat{u}_l} + \frac{l'\cdot p}{\hat{u}\hat{s}_l} + \frac{l'\cdot p'}{\hat{s}\hat{s}_l} \right) \\
& + l\cdot p\left[\frac{\hat{s}\hat{s}_l}{\hat{u}\hat{u}_l} - 3 \right. \\
& + \frac{2}{\hat{u}\hat{u}_l}(\hat{s}l'\cdot p + \hat{s}_l l\cdot p' - (\hat{u}+\hat{u}_l)l'\cdot p') \Bigg] \\
& + l\cdot p'\left[\frac{\hat{u}\hat{s}_l}{\hat{s}\hat{u}_l} - 3 \right. \\
& + \frac{2}{\hat{s}\hat{u}_l}(-\hat{s}_l l\cdot p - \hat{u}l'\cdot p' + (\hat{s}+\hat{u}_l)l'\cdot p) \Bigg] \\
& + l'\cdot p\left[\frac{\hat{s}\hat{u}_l}{\hat{u}\hat{s}_l} - 3 \right. \\
& + \frac{2}{\hat{u}\hat{s}_l}(-\hat{s}l\cdot p - \hat{u}_l l'\cdot p' + (\hat{u}+\hat{s}_l)l\cdot p') \Bigg] \\
& + l'\cdot p'\left[\frac{\hat{u}\hat{u}_l}{\hat{s}\hat{s}_l} - 3 \right. \\
& + \frac{2}{\hat{s}\hat{s}_l}(\hat{u}l\cdot p' + \hat{u}_l l'\cdot p - (\hat{s}+\hat{s}_l)l\cdot p) \Bigg] \Bigg\}.
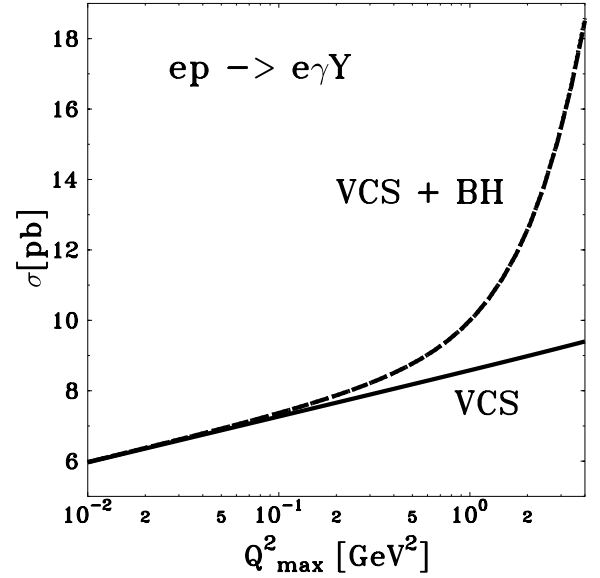\end{aligned}
\qquad (15)
$$

Fig. 6. Dependence of the total $ep \to e\gamma Y$ cross section on the maximal momentum transfer Q^2_{max}. The solid line shows the contribution of virtual Compton scattering (VCS, Fig. 5b) alone, while the dashed line includes also the Bethe–Heitler (BH, Fig. 5a) contribution and the interference term. The kinematic region is defined in the text

The results presented in (12)–(15) have previously been computed, e.g., in [26], but with our particular choice of kinematical variables we obtained more compact expressions.

In Fig. 6 we compare the VCS to the total VCS+BH cross section for $ep \to e\gamma Y$ as a function of Q^2_{max}, the maximum momentum transfer between the electrons. The differential cross section (10) was integrated over the ranges $x_s \in [0.01, 0.7]$, $W \in [40\,\mathrm{GeV}, 160\,\mathrm{GeV}]$, $\phi \in [0, 2\pi]$, $-t \in [4\,\mathrm{GeV}^2, 10\,\mathrm{GeV}^2]$, and $Q^2 \in [m_e^2, Q^2_{\mathrm{max}}]$[1].

3.3. The semi-exclusive cross section

We have found that the process $ep \to e\gamma Y$ can be used to study semi-exclusive photon production at HERA in the kinematic range $W^2/M_Y^2 \gtrsim 10$, $Q^2 \lesssim 0.1\,\mathrm{GeV}^2$ and $-t \gtrsim 4\,\mathrm{GeV}^2$. In Fig. 7 we show the cross section

$$
\begin{aligned}
\frac{\mathrm{d}\sigma(ep \to e\gamma Y)}{\mathrm{d}(W^2/M_Y^2)} = {}& \int_{0.25}^{0.75} \mathrm{d}y\, f_{\gamma/e}(y, Q^2_{\mathrm{max}} = 0.1\,\mathrm{GeV}^2) \\
& \times \int_{|t|_{\mathrm{min}}}^{|t|_{\mathrm{max}}} \mathrm{d}t \frac{-t(1-x_s)^2}{W^2} \sum_{i \in q,g} f_{i/p}(x_s, -t)\frac{\mathrm{d}\sigma}{\mathrm{d}t}(\gamma i \to \gamma i)
\end{aligned}
\qquad (16)
$$

for two ranges of momentum transfer, $4\,\mathrm{GeV}^2 < -t < 10\,\mathrm{GeV}^2$ and $10\,\mathrm{GeV}^2 < -t < 30\,\mathrm{GeV}^2$. The full curve

---

[1] In order to ensure that the electron propagators are far off-shell we also required $\hat{s}_l, -\hat{u}_l > -t_{\mathrm{min}} = 4\,\mathrm{GeV}^2$. This cut is, however, irrelevant for $Q^2 \lesssim 1\,\mathrm{GeV}^2$
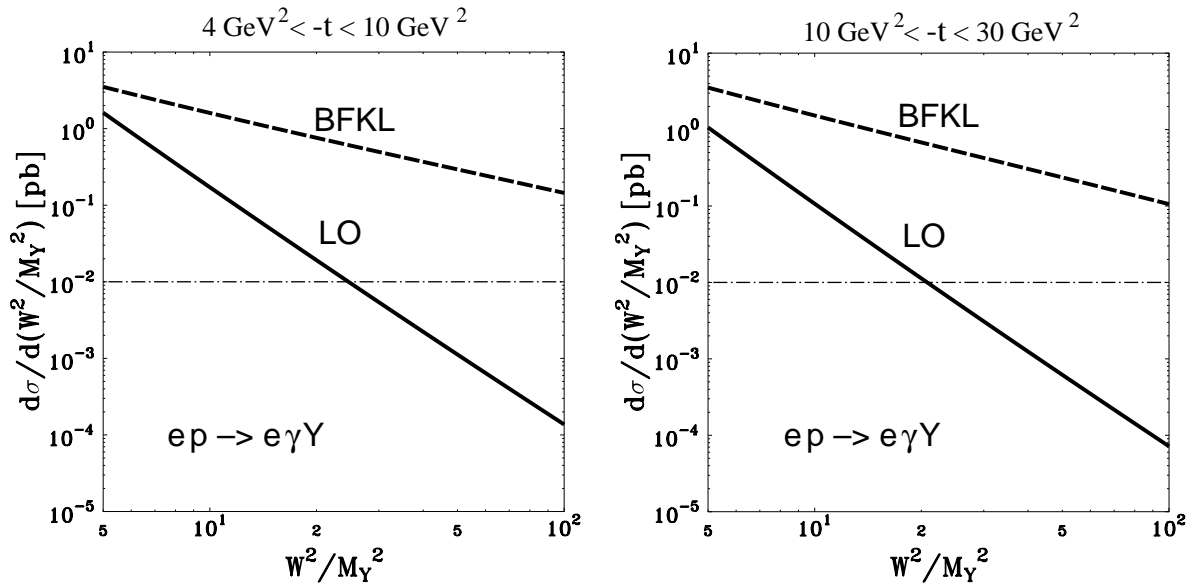
Fig. 7. The cross section $\mathrm{d}\sigma(ep \to e\gamma Y)/\mathrm{d}(W^2/M_Y^2)$ of (16) shown for two ranges of t: $4\,\mathrm{GeV}^2 < -t < 10\,\mathrm{GeV}^2$ (left) and $10\,\mathrm{GeV}^2 < -t < 30\,\mathrm{GeV}^2$ (right). The solid line shows the contribution of the LO process of (3) (Fig. 2a). The dashed line shows that of the BFKL process of (17) (Fig. 2c plus gluon ladder iterations). The horizontal dash-dotted line gives the 1 event level per unit of W^2/M_Y^2, for a HERA luminosity of 100 events/pb

shows the contribution of the LO process of (3) (Fig. 2a). The dashed curve shows the contribution of the BFKL subprocess of (6) (Fig. 2c, plus gluon ladder iterations), together with the corresponding $\gamma q \to \gamma q$ sea quark BFKL contribution [14],

$$\frac{\mathrm{d}\sigma_{\mathrm{BFKL}}}{\mathrm{d}x_s \mathrm{d}t} = \left[g(x_s, -t) + \frac{16}{81}\Sigma(x_s, -t) \right]$$
$$\times \frac{\mathrm{d}\sigma_{\mathrm{BFKL}}}{\mathrm{d}t}(\gamma g \to \gamma g) , \qquad (17)$$

where Σ denotes the quark singlet distribution $\Sigma = \sum_q [f_{q/p} + \bar{f}_{q/p}]$. We use $\alpha_s = 0.2$ in the BFKL cross section and assume three (four) active flavors in the low (high) $|t|$-range. The horizontal dash-dotted line indicates the 1 event level per unit of W^2/M_Y^2, given a nominal HERA luminosity of 100 events/pb.

We should emphasize that the BFKL approximation may not be reliable for $W^2/M_Y^2 \lesssim 100$ [15]; hence the dashed curve is an extrapolation. It is nevertheless interesting to observe that this extrapolation dominates the LO $q\gamma \to q\gamma$ contribution over the whole semi-exclusive range $W^2/M_Y^2 \gtrsim 10$. This conclusion is insensitive to the t-range and also to the range of y (not shown).

4. Conclusions

Semi-exclusive processes $A + B \to C + Y$ provide a new tool for investigating hadron structure. Effective currents formed by the $A\overline{C}$ system generalize the virtual photon probe familiar from DIS and can carry charge, flavor, baryon and other quantum numbers [1]. Before this tool can be put to use, at least two questions need to be answered:

(i) How stringent should be the limits $\Lambda_{\mathrm{QCD}}^2 \ll -t, M_Y^2 \ll W^2$ which must be imposed in order for the semi-exclusive production mechanism to dominate?
(ii) Can the hard $A\overline{C}$ vertex be reliably computed using PQCD?

In this paper we studied the process $\gamma p \to \gamma Y$, which is especially simple in the sense that both particles A and C have a pointlike component. Based on simulations with the PYTHIA and LUCIFER event generators we concluded that semi-exclusive dynamics should dominate for $W^2/M_Y^2 \gtrsim 10$ and $-t \gtrsim 4\,\mathrm{GeV}^2$. Photon emission from the electron (the Bethe–Heitler process) is insignificant for incoming photon virtualities $Q^2 \lesssim 0.1\,\mathrm{GeV}^2$ and can be further suppressed with angular cuts. The semi-exclusive cross section should be measurable at HERA, assuming that the subprocess cross section $\hat{\sigma}(\gamma q \to \gamma q)$ is not smaller than its lowest order (LO) PQCD approximation.

Point (ii) above is non-trivial, since the semi-exclusive kinematics implies a high energy (Regge) limit for the subprocess, $\hat{s}/-t \gg 1$. Little is known about the importance of higher order (HO) PQCD corrections in this limit. In the process under study the situation is particularly intriguing since the LO subprocess diagrams shown in Fig. 2a,b correspond to $q\bar{q}$ exchange in the t-channel. At high subenergies $\hat{s}$ they are therefore suppressed by a factor $1/\hat{s}^2$ in the cross section compared to the $\mathcal{O}(\alpha_s^4)$ gluon exchange contribution of Fig. 2c. The latter is, on the other hand, just the first term in the series of gluon ladder diagrams which is supposed to build up the BFKL Pomeron in this process [13–15].

It is not clear from which value of $\hat{s}/-t$ HO contributions like Fig. 2c start to dominate the LO processes

of Fig. 2a,b. The BFKL approximation has been assumed to be relevant for $\hat{s}/-t \gtrsim 100$ [15]. Extrapolating the BFKL cross section to lower energies we found (Fig. 7) that it would in fact dominate the LO cross section in the whole range of semi-exclusive dynamics, $\hat{s}/-t \gtrsim 10$. The ratio σ_{HO}/σ_{LO} behaves approximately like $(\widetilde{W}^2/M_Y^2)^2$, closely reflecting the $\hat{s}/-t$-dependence of the respective subprocesses, cf. (9). A measurement of the $(W^2/M_Y^2)^2$-dependence of the cross section will thus directly determine the nature of the dominant t-channel exchange.

We conclude that the large HERA energy in principle allows accessing the semi-exclusive kinematic region, with its double hierarchy of large scales. The limiting factor will be the luminosity. If the cross section is approximately given by the lowest order contribution in Fig. 7, then only a restricted range of $(W^2/M_Y^2)^2$ can be studied. Since the higher order two gluon exchange (BFKL) contributions fall off more slowly with $(W^2/M_Y^2)^2$ they will eventually dominate. If their normalization is even close to that indicated by the BFKL extrapolation of Fig. 7, there should be a rich semi-exclusive phenomenology at HERA, not only for photon but also for meson (π, ρ, J/ψ) production. Further work is needed to estimate the feasibility of measuring charge exchange processes and the three gluon (Odderon) contribution to π^0 production.

References

1. S.J. Brodsky, M. Diehl, P. Hoyer, S. Peigne, Phys. Lett. B **449**, 306 (1999) [hep-ph/9812277]. For earlier related work, see C.E. Carlson, A.B. Wakely, Phys. Rev. D **48**, 2000 (1993)
2. T. Sjöstrand, Comput. Phys. Commun. **82**, 74 (1994)
3. G. Ingelman, A. Weigend, Comput. Phys. Commun. **46**, 241 (1987)
4. J. Breitweg et al. [ZEUS Collaboration], Phys. Lett. B **413**, 201 (1997) [hep-ex/9708038]; Phys. Lett. B **472**, 175 (2000) [hep-ex/9910045]
5. S.W. Lee [ZEUS collaboration], Nucl. Phys. Proc. Suppl. **82**, 162 (2000) [hep-ex/9911051]
6. D.W. Duke, J.F. Owens, Phys. Rev. D **26**, 1600 (1982); Erratum: Phys. Rev. D **28**, 1227 (1983)
7. P. Aurenche, A. Douiri, R. Baier, M. Fontannaz, D. Schiff, Z. Phys. C **24**, 309 (1984)
8. P. Aurenche, P. Chiappetta, M. Fontannaz, J.P. Guillet, E. Pilon, Z. Phys. C **56**, 589 (1992)
9. L.E. Gordon, Phys. Rev. D **57**, 235 (1998) [hep-ph/9707464]
10. M. Krawczyk, A. Zembrzuski, IFT 98/12, hep-ph/9810253
11. S. Frixione, Phys. Lett. B **429**, 369 (1998) [hep-ph/9801442]
12. I.F. Ginzburg, D.Y. Ivanov, Phys. Rev. D **54**, 5523 (1996) [hep-ph/9604437]
13. D.Y. Ivanov, M. Wüsthoff, Eur. Phys. J. C **8**, 107 (1999) [hep-ph/9808455]
14. N.G. Evanson, J.R. Forshaw, Phys. Rev. D **60**, 034016 (1999) [hep-ph/9902481]
15. B.E. Cox, J.R. Forshaw, hep-ph/9912486
16. A. Afanasev, C.E. Carlson, C. Wahlquist, Phys. Rev. D **58**, 054007 (1998) [hep-ph/9706522]
17. M.A. Doncheski, R.W. Robinett, Phys. Rev. D **46**, 2011 (1992)
18. E.L. Berger, E. Braaten, R.D. Field, Nucl. Phys. B **239**, 52 (1984)
19. J. Bartels, J.R. Forshaw, H. Lotter, M. Wüsthoff, Phys. Lett. B **375**, 301 (1996) [hep-ph/9601201]
20. ZEUS Collaboration, Study of the diffractive production of vector mesons at large Q^2 or at high $|t|$ at HERA, Contribution to the International Europhysics Conference on High Energy Physics, Tampere, Finland 1999. See also http://zedy00.desy.de/~schlenst/eps99_paper.html.
21. B. Cox, J. Forshaw, L. Lönnblad, JHEP **9910**, 023 (1999) [hep-ph/9908464]
22. V.S. Fadin, L.N. Lipatov, Phys. Lett. B **429**, 127 (1998) [hep-ph/9802290]
23. S. Frixione, M.L. Mangano, P. Nason, G. Ridolfi, Phys. Lett. B **319**, 339 (1993) [hep-ph/9310350]
24. S. Frixione, G. Ridolfi, Nucl. Phys. B **507**, 315 (1997) [hep-ph/9707345]
25. M. Glück, E. Reya, A. Vogt, Z. Phys. C **67**, 433 (1995)
26. S.J. Brodsky, J.F. Gunion, R. Jaffe, Phys. Rev. D **6**, 2487 (1972)